Journal of the Korean Society of Marine Environment & Safety
Research Paper
Vol. 30, No. 5, pp. 506-515, August 31, 2024, ISSN 1229-3431(Print) / ISSN 2287-3341(Online) https://doi.org/10.7837/kosomes.2024.30.5.506

Numerical Study on Effect of Longitudinal Center of Gravity (LCG) Changes on Cruise-Ship Resistance in Shallow Water

Michael* · Kwang-Cheol, Seo** · Kyoung-Woo, Lee**†
* Graduate School of Mokpo National Maritime University, Mokpo 58628, Korea
** Professor, Department of Naval Architecture & Ocean Engineering, Mokpo National Maritime University, Mokpo 58628, Korea

천수 효과를 고려한 무게중심과 수심 변화에 따른 유람선의 저항성능에 대한 전산유체역학 해석 연구

마이클* · 서광철** · 이경우**†
* 국립목포해양대학교 대학원, ** 국립목포해양대학교 조선해양공학과 교수

Abstract : *Owing to the interaction between a ship and the river bed, several phenomena resulting in increased resistance may have occurred. This increase in resistance is primarily due to the wave-making performance. Thus, this study aims to reduce the wave-making resistance by optimizing the performance of an electric canal cruise through changing the longitudinal center of gravity (LCG). Numerical simulations are performed to obtain the lowest resistance by optimizing the LCG position; subsequently, the effect of water depth is included as the next variable. Results show that LCG variations of 37.5% - 52.5% Lpp can result in a wide range of total resistance. In deep water, a 72.67% resistance gap is achieved by comparing the highest and lowest resistances, whereas a slightly lower gap of up to 62.97% is achieved in shallow water. Additionally, smaller water depths correspond to higher resistance. The resistance increased by a maximum of 67.68% in shallow water measuring 1.5 m, as compared with the case of deep water. This increase in resistance is primarily due to wave-making resistance, which constitutes 84.99% of the total resistance.*

Key Words : *Longitudinal center of gravity (LCG), Shallow-water effect, Resistance, Wave-making resistance, Numerical analysis*

요 약 : 얕은 물에서 선박과 바닥의 상호작용으로 인해, 제한이 없는 깊은 물에서 운항할 때와 비교하여 저항이 증가하는 현상이 발생한다. 이러한 천수효과에 의해 증가하는 저항은 주로 조파저항에 기인하기 때문에, 본 연구에서는 유람선을 대상으로 LCG(Longitudinal Center of Gravity)의 위치 변경을 통해 성능을 최적화하여 조파저항을 감소시키는 것을 목표로 진행하였다. 수치해석 시뮬레이션을 통해 LCG 위치를 최적화하여 저항의 최소값을 찾고, 이후 수심의 깊이에 따른 영향을 분석하였다. 분석 결과, 37.5% - 52.5% Lpp의 영역에서의 LCG 변화는 총 저항에 큰 영향을 주었으며, 깊은 물의 조건에서는 총 저항의 최대값과 최소값을 비교하였을 때, 72.67%의 큰 차이를 보이는 반면, 얕은 물 조건에서는 그 차이가 62.97% 정도로 비교적 낮은 차이를 보인다. 수심의 깊이에 따른 효과는 수심이 낮을수록 총 저항이 증가하는 경향을 보였다. 깊은 물과 비교하여 1.5m의 얕은 물에서는 총 저항이 최대 67.68% 가량 증가하는 것으로 분석되었다. 이 경우 총 저항 증가의 주요 원인은 전체 저항의 84.99%를 차지하는 조파저항에 의한 것으로 판단된다.

핵심용어 : LCG, 천수효과, 저항성능, 조파저항, 수치해석

1. Introduction

International Maritime Organization (IMO) has a global goal to reach net zero for CO2 emissions by 2050 (IMO, 2023), therefore, several efforts have been made including alternative fuels such as electric ships. In total, the electric ship market is estimated to have a total value of around USD 3.41 billion in 2023, which is projected to increase by up to 12.87 billion in 2030, with an average Compound Annual Growth Rate (CAGR) of 18.9% (Fortune Business Insights, 2024). Implementing electric batteries as an alternative fuel for ships is more possible in relatively

* First Author : michael.navarc@gmail.com
† Corresponding Author : kwlee@mmu.ac.kr, 061-240-7307

small-size ships (Chatelier, 2023). Small-size ships are not commonly designed as seagoing ships, however in smaller water regions such as inland waterways like rivers, or lakes. However, the design of seagoing ships and inland ships is to be considered, since there are some limitations such as water depth. In fact, a low-draught vessel is required to accommodate the clearance of water depth to avoid the ship's grounding.

Several phenomena are believed to have happened due to the interaction of the ship and the river bed. Water speed might increase around the hull, along with the pressure gradients, as the hull interacts with the seabed (Hoa et al., 2019). The wave pattern also differs between deep and shallow water, which leads to a change in wave-making resistance (Prakash and Chandra, 2013). At critical speed defined by depth Froude Number equal to 1.0 (Fn_H = 1.0), solitary waves are created and travel slightly faster in the bow section, leading to oscillations in the vertical axis and a significant increase in wave resistance (Patel and Premchand, 2015). An increase of total resistance by up to 110.80% is estimated by CFD simulations in the H/T ratio of 1.5 compared to the unrestricted water depth (Pacuraru and Domnisoru, 2017). The increase of resistance near the critical depth Froude Number is significant due to the smaller clearance under the ship's keel, which is proven by towing test experiments (Molland et al., 2004), having two water depths analyzed along with several speeds of length Froude Number of 0.25 - 1.0, resulting in depth Froude Number of 0.5 - 3.0. The interesting result to be noted is that, at the higher Fn, the resistance results for both unrestricted water and shallow water are quite similar, despite the significant difference of the wave patterns.

Understanding the phenomenon of the increase of the resistance is mainly due to the wave-making performance, this study aims to reduce the resistance of wave-making performance by optimizing the ship's performance by changing the Longitudinal Center of Gravity. Several studies have proven that LCG, trim optimization, and loading conditions are the efforts that can be made to reduce wave-making resistance (Kim et al., 2009), (Le et al., 2021), (Lim et al., 2023). A recent study of numerical and empirical shows that the LCG changes could lead to a total resistance reduction by up to 45%, which is dominated by the reduction of pressure resistance components by up to -23% (Michael et al., 2023).

Combining these two factors of LCG and water depth, this study aims to utilize numerical simulations to understand the effect of water depth on the increase of the resistance, which aims to be countered by lowering the resistance, by LCG changes. In hopes, that a better resistance performance of a shallow water canal cruise design can be created.

2. Methodology

Numerical simulations will be conducted using Computational Fluid Dynamics (CFD) along with the guidelines and recommendations (ITTC, 2014) to evaluate the effect of shallow water and LCG changes on the resistance performance of the canal cruise ship.

2.1 Target Vessel

A 14 m-long monohull of shallow draft electric cruise designed and operated in a canal became the target vessel of this study. With a design speed of 3.0 - 7.0 knots, the vessel has a speed Froude Number of 0.13 - 0.31. The bare hull's principal dimensions and linesplan are detailed and summarized in Table 1, and Fig. 1. as follows. The vessel has a relatively shallow draft of 0.5 m due to the water depth limitations of the canal, making it in total has a displacement of about 14 tons.

Table 1. Target vessel's principal dimensions

Principal Dimensions	Value	Units
Length overall	14.84	m
Breadth	3.50	m
Draft	0.50	m
Speed	3.0 - 7.0	knots
Froude number	0.13 - 0.31	-
Displacement	14.72	ton

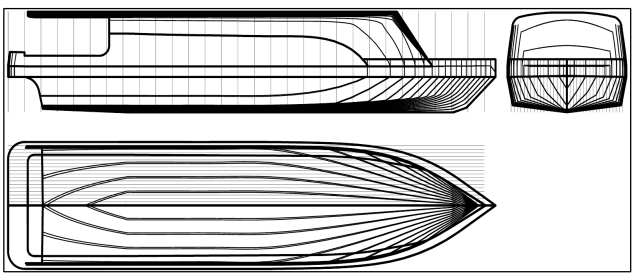

Fig. 1. Target vessel's linesplan.

2.2 Scope of Study

The numerical study means to see the effect of water depth on the resistance performance. Since shallow water could lead to an increase in the resistance, this study also aims to counter the increment of resistance by means of LCG changes in order to optimize trim conditions.

Seven different LCG points are considered in 2 different water depths, and 1 speed, making in total of 14 study cases for the LCG changes, as summarized in Table 2. In addition to water depth analysis, in total of 4 water depths, and 5 different speeds are considered, making it in total of 20 more study cases in this study, as summarized in Table 3. In total, 34 numerical simulations are to be performed, summarized in Table 2 and Table 3, and illustrated in Fig. 2.

Table 2. LCG range of study, speed at 7 knots

LCG	Water Depth	
(% L_{PP})	Deep	1.50 m
37.5	Case #1	Case #8
40.0	Case #2	Case #9
42.5	Case #3	Case #10
45.0	Case #4	Case #11
47.5	Case #5	Case #12
50.0	Case #6	Case #13
52.5	Case #7	Case #14

Table 3. Water depth and speed range of study, LCG at 50.0%

Speed		Water Depth			
Knots	Froude	Deep	3.50 m	2.50 m	1.50 m
3	0.132	#15	#16	#17	#18
4	0.176	#19	#20	#21	#22
5	0.219	#23	#24	#25	#26
6	0.263	#27	#28	#29	#30
7	0.307	#31	#32	#33	#34

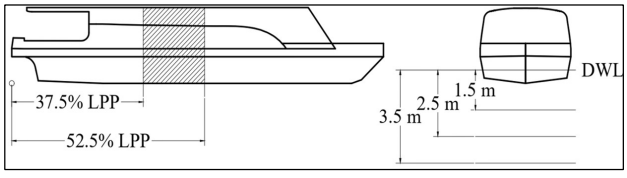

Fig. 2. Scope of study of LCG changes (left), and water depth (right).

3. Numerical Simulations

Due to the computational costs of towing test experiments, numerical simulations are used in this study. In this study, Computational Fluid Dynamics (CFD) commercial software of Simcenter Star-CCM+ is used.

3.1 Methodologies

Based on several references that have been summarized, the same methodologies will be applied in this study. The governing equations for the incompressible flow chosen in this study are the Reynolds-averaged Navier-Stokes (RANS) equation, along with the implicit unsteady time-step model. The equation is represented as follows:

$$\frac{dV}{dt}+\oint_{S(t)} dS \cdot (u-v)=0 \tag{1}$$

where dV and dt are the volume element and time control, S and dS are the surface vector and surface area element, u is the velocity vector, and v is the velocity resulting from the motion of the volume control. While the conversation in momentum and stress tensor is presented as follows, where T is the stress, P is the pressure, I is the identity, ∇u is the gradient of u, and $(.)^T$ is the transpose factor.

$$\frac{d}{dt}\int_{V(t)} u\,dV=\oint_{S(t)} dS \cdot \overline{T} \tag{2}$$

$$\overline{T}=-(u-v)u-P\bar{I}+v\left[\nabla u+(\nabla u)^T\right] \tag{3}$$

Turbulence flow is modeled by the SST-$k-\omega$ model, which can give a better accuracy within the boundary layer, and leads to better and more accurate resistance prediction by simulating the flow separation better. The following equations of SST-$k-\omega$ is presented as follows:

$$\frac{D\rho k}{Dt}=\tau_{ij}\frac{\delta u_i}{\delta x_j}-\beta^*\rho\omega k+\frac{\delta}{\delta x_j}\left[(\mu+\sigma_\omega\mu_t)\frac{\delta_\omega}{\delta x_j}\right] \tag{4}$$

$$\frac{D\rho\omega}{Dt}=\frac{\Upsilon}{v_t}\tau_{ij}\frac{\delta u_i}{\delta x_j}-\beta\rho\omega^2+\frac{\delta}{\delta x_j}\left[(\mu+\sigma_\omega\mu_t)\frac{\delta\omega}{\delta x_j}\right] +2\rho(1-F_1)\sigma_{\omega 2}\frac{1}{\omega}\frac{\delta k}{\delta x_j}\frac{\delta\omega}{\delta x_j} \tag{5}$$

Several constants used in equations (4) and (5) above are to modify the $k-\epsilon$ model to $k-\omega$ models, as follows:

$\sigma_{\omega 1}=0.5, \beta_1=0.075, \beta^*=0.09, \kappa=0.41, \sigma_{k2}=1.0, \sigma_{\omega 2}=0.856,$
$\beta_2=0.0828, \gamma_1=\beta_1/\beta^*-\sigma_{\omega 1}\kappa^2/\sqrt{\beta^*}, \gamma_2=\beta_2/\beta^*-\sigma_{\omega 2}\kappa^2/\sqrt{\beta^*}$

The interaction of water and air in the free surface area is modeled with the Volume of Fluid (VOF) method. In the free surface, High-Resolution Interface Capturing (HRIC) is applied. The air is modeled as light fluid, and freshwater as the heavy fluid. With the notation of F as the volume fraction, the air is notated as 0, and water is 1, where the interface is in between (0 < F < 1).

Two degrees of freedom are used to simulate the cruise motion, namely heave, and pitch. Therefore, the Dynamic Fluid Body Interaction (DFBI) is used. The DFBI node becomes one of the important options in this study due to the LCG changes performed under this setting.

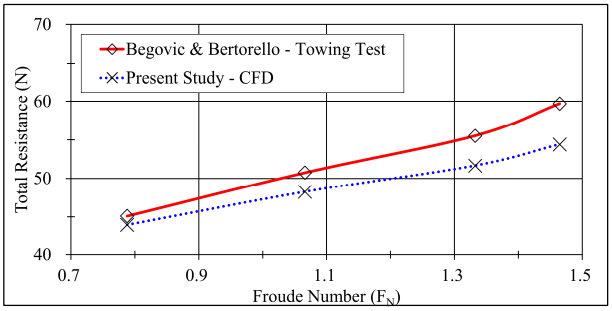

Fig. 3. Validations of numerical simulations methodologies (resistance).

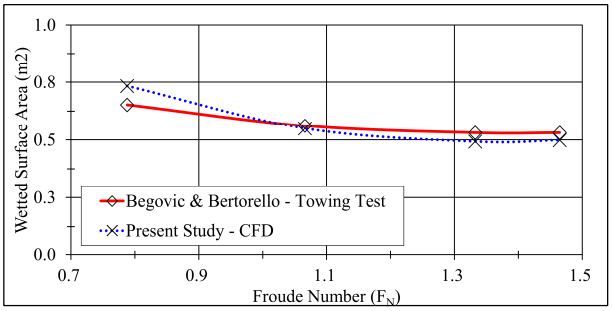

Fig. 4. Validations of numerical simulations methodologies (wetted surface area).

For the verification of methodologies used in this study, a verification process is performed. Therefore, a warped-2 hull form is used (Begovic and Bertorello, 2012). The warped-2 hull form consists of the results of the experiment towing test, along with the details of hull geometry and 3D model.

The results are presented in Fig. 3. and Fig. 4. where the resistance and wetted surface area are the factors that are chosen to be verified. The total resistance predicted by the CFD method differs slightly in average of 5.81%, while the wetted surface for about 6.97%.

3.2 Computational Domain, Boundaries, and Regions

Verified methodologies mentioned in the previous section are applied to the computational domain, boundaries, and regions to perform mesh convergence studies. The domain is designed considering the computational time, notated with a notation of L as the cruise's overall length. The recommendations of ITTC (ITTC, 2014) are also taken into consideration, and the final virtual towing tank along with the size is presented in Fig. 5. below. It is worth mentioning that the bottom regions are set to velocity inlet to capture the wave resistance better due to the reverse flow produced by the squat effect of shallow water.

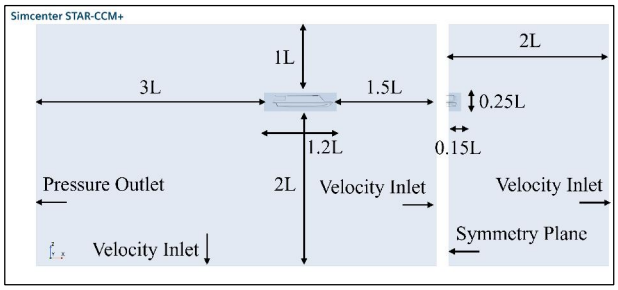

Fig. 5. Computational domain and regions (deep water)

3.3 Mesh Convergence Studies

The mesh convergence studies are started by y^+ studies. In this study, all y^+ treatment is used since it covers both coarse and fine mesh in the domain regions, and overset regions, respectively. Along with the ITTC recommendations (ITTC, 2014), 15 prism layers are used, and the y^+ target is set to be around greater than 40 as presented in Fig. 6. to fulfill the recommendations ($30 < y^+ < 100$). The desired y^+ has been chosen, Cf is the skin friction coefficient estimated by assuming the boundary layer on a flat plate with zero pressure gradient, followed by L as the length, and Re as Reynold's number. The first layer thickness of y, is determined with the equation (6).

$$y=\frac{y^+L}{Re_L\sqrt{\frac{C_f}{2}}} \tag{6}$$

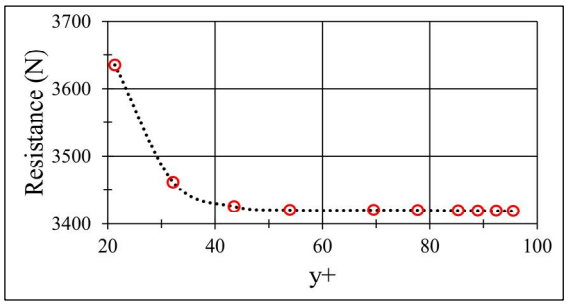

Fig. 6. y^+ convergence studies in boundary layers.

After determining the y^+, the size of cells is then studied by implementing Richardson's Extrapolation (Richardson, 1927). The idea is to compare the grid spacing of the numerical results to the assumed zero-spacing grid system. Three different mesh configurations namely fine, medium, and coarse are used, and the study results are summarized in Table 4. With a refinement factor around $\sqrt{2}$, along with some volume refinement, the Grid Convergence Index (GCI) is used to validate the accuracy of each mesh size.

Table 4. Mesh configurations study

Mesh	Cells (mil.)	RT (N)	f0	GCI_{12} (%)	GCI_{23} (%)
Fine	3.76	3,475			
Medium	2.69	3,529	3,437	1.36	3.26
Coarse	1.89	3,672			

As can be seen in Fig. 7. fine mesh configuration has a difference of 1.11% compared to the zero-grid spacing of Richardson's extrapolation. However, due to computational time considerations, the medium mesh as presented in Fig. 8. is chosen in this study, with a relatively higher difference, which is about 2.68% compared to the zero-grid spacing. These results are still considered satisfactory, knowing the GCI index of 1.36% between the fine and medium mesh configurations.

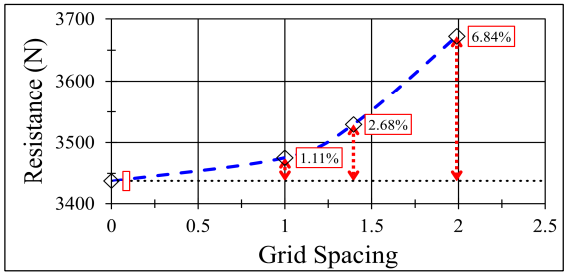

Fig. 7. Mesh size studies.

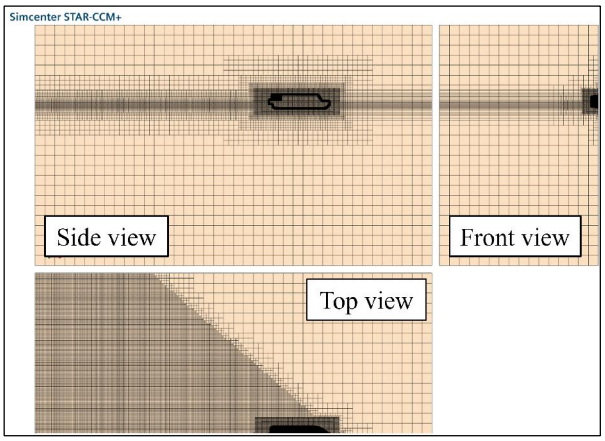

Fig. 8. Mesh configurations with volume refinement along overset, free surface, and wake regions.

4. Results

Two main variables are to be presented in this study. The first one, for the LCG changes, was studied in cases 1 – 14, and the second is for the water depth effect, was studied in the case 15 – 34. Both analyses are conducted following the numerical simulation procedure mentioned in the previous section.

4.1 LCG Changes

Using the numerical simulations, the LCG changes can be simulated under the DFBI options, which include the center of gravity of a body with a mass. The center of gravity is changed as the LCG shifted along in each case, while the mass is set to be the canal cruise's designed displacement mentioned in Table 1. Operating in 7 knots, along the LCG changes, both deep and shallow water of 1.5 m in fact give the same results, where the optimum LCG is located at 50.0% Lpp from the transom, knowing the fact that shifting the LCG further to 52.5% Lpp could lead to deck wetness due to bow trim, and in fact, increase the resistance. Having the LCG located at 37.5% Lpp gives the worst resistance performance for both cases of deep and shallow water of 1.5 m. The results are plotted into a graph presented in Fig. 9. and summarized in Table 5.

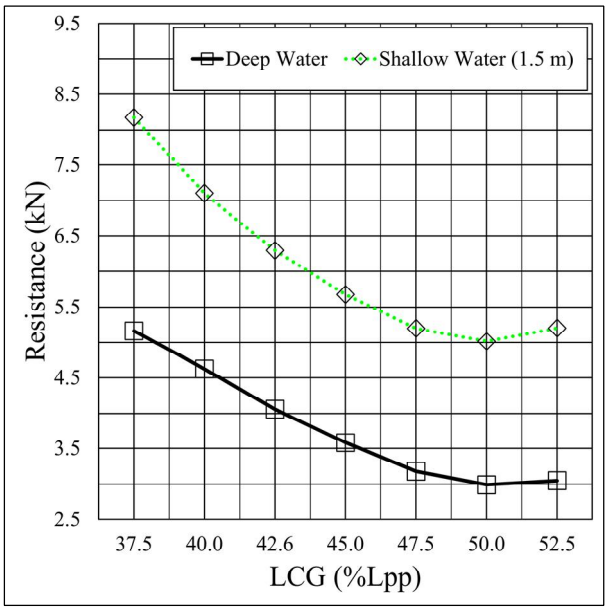

Fig. 9. Resistance changes due to LCG position, in deep water and shallow water of 1.5 m at 7 knots.

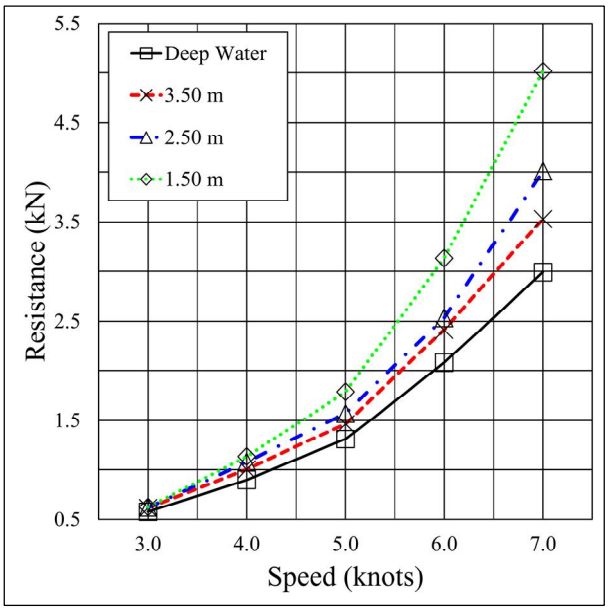

Fig. 10. Resistance changes due to water depth, in speed range of 3 - 7 knots, at LCG 50% Lpp.

Table 5. Numerical simulations results of resistance due to LCG changes (case 1 – 14)

LCG	Total Resistance (N)	
(% L_{PP})	Deep Water	1.50 m
37.5	5,146.96	8,173.86
40.0	4,618.42	7,101.70
42.5	4,057.38	6,290.66
45.0	3,578.66	5,674.54
47.5	3,178.04	5,200.02
50.0	2,991.24	5,015.70
52.5	3,047.22	5,203.02

Table 6. Numerical simulations results of resistance due to water depth and speed changes, LCG at 50.0% (case 15 – 34)

Speed	Resistance (N)			
Knots	Deep	3.50 m	2.50 m	1.50 m
3	579.07	617.92	621.69	627.08
4	899.27	1,003.67	1,078.04	1,132.24
5	1,307.20	1,464.19	1,570.47	1,785.58
6	2,079.20	2,414.16	2,534.54	3,129.94
7	2,991.24	3,527.57	4,006.17	5,015.70

4.2 Water Depth Effect

The water depth effect is simulated by the geometry size of the domain regions. As illustrated in Fig. 5, the bottom region size of 2L is subject to change according to the water depth. The LCG is set to be in the lowest resistance position mentioned in Table 5, which is at 50.0% Lpp (cases 6 and 13). The speed is set in the velocity of the flat wave under the physics settings of the Volume of Fluid (VOF). The results are plotted into a graph as presented in Fig. 10. and summarized in Table 6.

5. Discussions

Two main discussions are to be discussed in this study. The first one is for the LCG changes and the second is the water depth effect. This section aims to see the main idea of resistance changes due to these factors.

5.1 LCG Changes Effect

Summarized in Table 5, and presented in Fig. 9, the optimum LCG is located in 50.0% Lpp or cases 6 and 13. The resistance increment is then compared within cases 6 and 13 as the base. The analysis is presented in Fig. 11. for the changes, notated in

percentages. As summarized in Table 7, and 8, the increment of resistance is up to 72.67% in the deep water, and up to 62.97% in the shallow water of 1.50 m. Therefore, the LCG is proven as one of the important factors in this canal cruise resistance performance, since improper LCG changes could lead to significant total resistance, both in deep and shallow water.

Table 7. Total resistance changes due to LCG changes of deep water (case 1 - 7), at 7 knots

Case	LCG	Total Resistance (N)	
(#)	(% L_{PP})	Deep Water	Changes (%)
1	37.5	5,146.96	+72.67
2	40.0	4,618.42	+54.40
3	42.5	4,057.38	+35.64
4	45.0	3,578.66	+19.64
5	47.5	3,178.04	+6.24
6	50.0	2,991.24	-
7	52.5	3,047.22	+1.87

Table 8. Total resistance changes due to LCG changes of deep water (case 8 - 14), at 7 knots

Case	LCG	Total Resistance (N)	
(#)	(% L_{PP})	1.50 m	Changes (%)
8	37.5	8,173.86	+62.97
9	40.0	7,101.70	+41.59
10	42.5	6,290.66	+25.42
11	45.0	5,674.54	+13.14
12	47.5	5,200.02	+3.67
13	50.0	5,015.70	-
14	52.5	5,203.02	+3.73

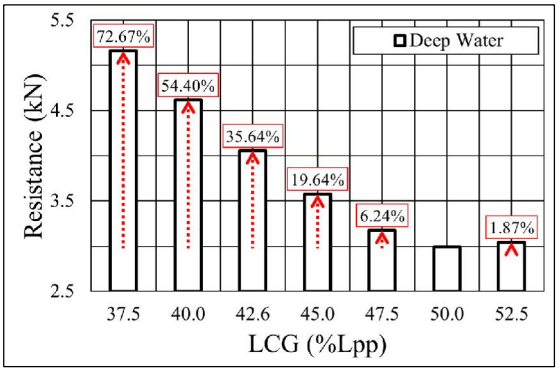

(a) in deep water

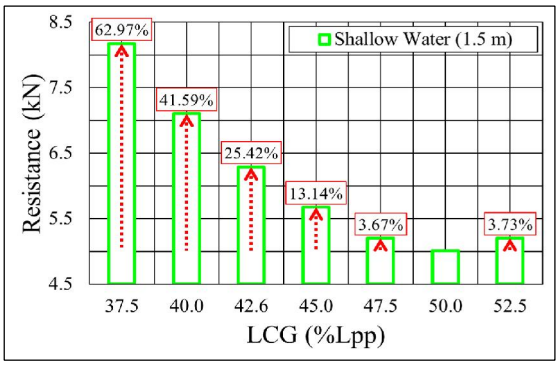

(b) in shallow wawter 1.5m

Fig. 11. Resistance variations due to LCG position.

5.2 Water Depth Effect

Summarized in Table 6, and presented in Fig. 10, the resistance increases as the water depth is decreased. The underwater clearance gives a significant rise in the total resistance. Also, as the speed gets higher, the increase of resistance is also significantly increased as well. Knowing the results of resistance is 579.07 N for case 15 at 3 knots for deep water, increase to 627.08 N for case 18 at the same speed, for shallow water of 1.5 m. However, at 7 knots, the increment significantly arises, knowing the results of resistance is around 2,991.4 N for deep water and 5,015.70 N for shallow water of 1.50 m.

The changes in resistance notated in percentage are to be summarized in Table 9. As can be seen in Fig. 12. on average, the increase of resistance is getting higher, as the water depth is getting lower. At the speed of 3 knots, compared to the deep water condition, the total resistance increases for about 6.71%, 7.36%, and 8.29%, for shallow water 3.5 m, 2.5 m, and 1.5 m, respectively, which is still considered not significant. However, compared to the speed of 7 knots, the total resistance increases by about 17.93%, 33.93%, and 67.68% for shallow water 3.5 m, 2.5 m, and 1.5 m, respectively, which can be concluded as significant.

Table 9. Total resistance changes due to water depth and speed changes, LCG at 50.0% (case 15 - 34)

Speed	3.50 m		2.50 m		1.50 m	
	RT	Change	RT	Change	RT	Change
(knot)	(N)	(%)	(N)	(%)	(N)	(%)
3	617.9	+6.71	621.7	+7.36	627.1	+8.29
4	1,004	+11.61	1,078	+19.88	1,132	+25.91
5	1,464	+12.01	1,570	+20.14	1,786	+36.60
6	2,414	+16.11	2,535	+21.90	3,130	+50.54
7	3,528	+17.93	4,006	+33.93	5,016	+67.68

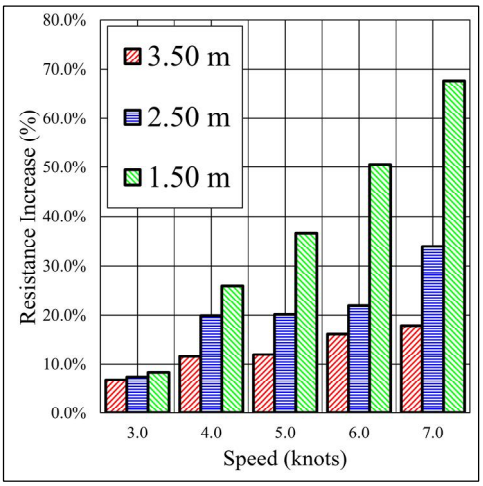

Fig. 12. Resistance increase compared to the deep water condition.

5.3 Shear and Pressure Components of Resistance

Shear force components consist of the tangential force acting on the wetted surface of the canal cruise. In this study, it is proven that LCG changes result in different wetted-surface areas, due to the different conditions of trim. Along with the speed changes, the wetted surface area is dynamically changed due to the uneven area of the bow and stern.

Besides, pressure components arise not only because of the viscosity of the water, and wetted surface area of the cruise but to the wave-making resistance. Various trim angles due to LCG changes result in different wave and wake patterns, which result in different wave-making contours.

This section aims to understand the portion of shear and pressure components to the total resistance. Therefore, the trend can be seen and analyzed for each case performed in this study. For cases 1 – 14, with LCG changes as the variable, the results are summarized in the table below.

From Table 10, it can be seen that the LCG changes mainly affect the pressure components of the total resistance. As an example, taking the case of deep water, where the total resistance ranges from 3.05 – 5.16 kN, the shear is actually increased from 0.59 to 0.73 kN. However, it is greatly countered by the reduction of wave-making resistance, by 4.57 kN to 2.27 kN in cases 1 to 7. This analysis proves that the LCG can change the resistance performance, by reducing the wave-making resistance or pressure components of the resistance. The same analysis is applied to the shallow water, where the resistance reduction is also achieved by reducing the wave-making resistance from 7.51 kN to 4.26 kN at cases 8 to 13.

Table 10. Shear and pressure components of total resistance, due to LCG changes (case 1 - 14)

Case	LCG	R_T	Shear		Pressure	
		Deep Water				
(#)	(% L_{PP})	(kN)	(kN)	(%R_T)	(kN)	(%R_T)
1	37.5	5.16	0.59	11.48	4.57	88.52
2	40.0	4.62	0.62	13.42	4.00	86.58
3	42.5	4.06	0.67	16.63	3.38	83.37
4	45.0	3.58	0.68	19.10	2.90	80.90
5	47.5	3.18	0.72	22.54	2.46	77.46
6	50.0	2.99	0.72	24.19	2.27	75.81
7	52.5	3.05	0.73	23.89	2.32	76.11
		Shallow Water 1.5 m				
8	37.5	8.17	0.66	8.13	7.51	91.87
9	40.0	7.10	0.67	9.48	6.43	90.52
10	42.5	6.29	0.69	10.99	5.60	89.01
11	45.0	5.67	0.71	12.46	4.97	87.54
12	47.5	5.20	0.73	13.99	4.47	86.01
13	50.0	5.02	0.75	15.01	4.26	84.99
14	52.5	5.20	0.76	14.65	4.44	85.35

In the case of 15 – 34, with water depth and speed as the variable, the wave-making resistance due to speed increases significantly in shallow water. Case 18 at the speed of 3 knots, has pressure components of 70.19%, and case 34, at the speed of 7 knots, has a significant increase of up to 82.03%. Therefore, speed is critical in this water depth, since it affects the wave-making resistance sensitively, compared to the deep water which gives no significant difference of 73.44% at case 15, to 75.81% at case 15 and case 31, for speeds 3 knots and 7 knots, respectively.

The results are shown in Table 11 below, which shows that in deep water cases, the total resistance consists of 24.19 – 28.41% of shear force, and 71.59 – 75.81% of pressure force, making it an average of 26.5% and 73.5% for shear and pressure forces. However, for the shallow water of 1.50 m, the total resistance consists of 15.01 – 29.81% of shear force, and 70.19 – 84.99% of pressure forces, making it an average of 22.1% and 77.9% for shear and pressure forces.

Table 11. Shear and pressure components of total resistance, due to water depth and speed changes (case 15 - 34)

Case	R_T	Shear		Avg.	Pressure		Avg.
Deep Water							
(#)	(kN)	(kN)	(%R_T)	(%)	(kN)	(%R_T)	(%)
15	0.58	0.15	26.56		0.43	73.44	
19	0.90	0.25	27.72		0.65	72.28	
23	1.31	0.37	28.41	26.5	0.94	71.59	73.5
27	2.08	0.53	25.62		1.55	74.38	
31	2.99	0.72	24.19		2.27	75.81	
Shallow Water 3.50 m							
16	0.62	0.16	26.33		0.46	73.67	
20	1.00	0.26	25.80		0.74	74.20	
24	1.46	0.39	26.73	24.5	1.07	73027	75.5
28	2.41	0.55	22.60		1.87	77.40	
32	3.53	0.73	20.83		2.79	79.17	
Shallow Water 2.50 m							
17	0.62	0.17	27.70		0.45	72.30	
21	1.08	0.27	25.03		0.81	74.97	
25	1.57	0.39	25.05	23.6	1.18	74.95	76.4
29	2.53	0.55	21.87		1.98	78.13	
33	4.01	0.74	18.56		3.26	81.44	
Shallow Water 1.50 m							
18	0.63	0.19	29.81		0.44	70.19	
22	1.13	0.28	24.86		0.85	75.14	
26	1.79	0.41	22.68	22.1	1.38	77.32	77.9
30	3.13	0.56	17.97		2.57	82.03	
34	5.02	0.75	15.01		4.26	84.99	

6. Conclusions

Understanding the analysis for two main variables of LCG and water depth changes to the total resistance of canal cruise by numerical simulations, several conclusions can be summarized, as follows:

1. LCG is one of the sensitive factors to consider for resistance performance. Knowing the fact that a gap of up to 72.67% is achieved in deep water, and 62.97% in shallow water 1.5 m, when comparing the highest and lowest resistance for all LCG positions. The main reason why the LCG can reduce the resistance is by reducing pressure components, or wave-making resistance. Therefore, the effect of LCG is more sensitive and effective in deep water. This can happen due to the fact that there is no interaction between the cruise ship to the waterbed at the deep water, so the wave-making resistance is dependent on the LCG. In the case of shallow water, the wave-making resistance reduction is not only affected by the LCG changes but also the interaction of the canal cruise's bottom section to the seabed, making it not as efficient as the deep water condition.
2. Water depth can significantly increase the resistance. As the water depth is reduced from deep water to shallow water, the resistance is increased by about 17.93, 33.93, and 67.68% for water depths 3.50, 2.50, and 1.50 m, respectively. These results also proved that the higher the speed, the lower the water depth, the higher the increment of the resistance.
3. Speed is critical and affects the shear and pressure components in the case of shallow water compared to deep water. Knowing the results of deep water gives a variation of 24.19 – 28.41% for the shear forces, compared to the shallow water of 1.50 m which gives variations of 15.01 – 29.81% for shear force.

Acknowledgement

This research was supported by "Regional Innovation Strategy (RIS)" through the National Research Foundation of Korea(NRF) funded by the Ministry of Education(MOE)(2021RIS-002).

References

[1] Begovic, E. and C. Bertorello(2012), Resistance assessment of warped hullform. Ocean Engineering, Vol. 56, pp. 28-42.

[2] Chatelier, J. M.(2023), Entering a new era for electrical vessel on inland waterways. Ship Science & Technology, 16(32), pp. 21-32.

[3] Fortune Business Insights(2024), [Online] Available at: https://www.fortunebusinessinsights.com/electric-ships-market-104444.

[4] Hoa, N. T. N., V. N. Bich, T. N. Tu, N. M. Chien, and L. T. Hien(2019), Numerical investigating the effect of water depth on ship resistance using RANS CFD method. Polish Maritime Research, 26(3), pp. 56-64.

[5] IMO(2023), 2023 IMO Strategy on Reduction of GHG Emissions from Ships, s.l.: Marine Environment Protection Committee, MEPC.377(80).

[6] ITTC(2014), ITTC - Recommended Procedures and Guidelines - Practical Guidelines for Ship CFD Applications (7.5-03-02-03), s.l.: International Towing Tank Conference.

[7] Kim, D. -J., K. -P. Rhee, and H. -S. Park(2009), A study on the effects of weight and center of gravity of a planning craft on running attitude. Journal of the Society of Naval Architects of Korea, 46(3), pp. 335-342.

[8] Le, T. H. M. T. Vu, V. N. Bich, N. K. Phuong, N. T. H. Ha, T. Q. Chuan, and T. N. Tu(2021) Numerical investigation on the effect of trim on ship resistance by RANSE method. Applied Ocean Research, Vol. 111, 102642.

[9] Lim, J.-T., Michael, N. -K. Im, and K. -C. Seo(2023), Study of small craft resistance under different loading conditions using model test and numerical simulations. Journal of the Korean Society of Marine Environment & Safety, 29(6), pp. 672-680.

[10] Michael, J. -T. Lim, N. -K. Im, and K. -C. Seo(2023), Empirical and numerical analyses of a small planing ship resistance using longitudinal center of gravity variations. Journal of the Korean Society of Marine Environment & Safety, 29(7), pp. 971-979.

[11] Molland, A. F., P. A. Wilson, D. J. Taunton, S. Chandraprabha, and P. A. Ghani(2004), Resistance and wash wave measurements on a series of high speed displacement monohull and catamaran forms in shallow water. International Journal of Maritime Engineering, Vol. 146, p. 15.

[12] Pacuraru, F. and L. Domnisoru(2017), Numerical investigation of shallow water effect on a barge ship resistance. IOP Conference Series: Materials Science and Engineering, 227, 012088.

[13] Patel, P. K. and M. Premchand(2015), Numerical investigation of the influence of water depth on ship resistance. International Journal of Computer Applications, 116(17), pp. 10-17.

[14] Prakash, S. and B. Chandra(2013), Numerical estimation of shallow water resistance of a river-sea ship using CFD. International Journal of Computer Applications, 71(5), pp. 33-40.

[15] Richardson, L. F.(1927), The deferred approach to the limit. Transactions of the Royal Society of London, Vol. 226, pp. 299-361.

Received : 2024. 07. 09.
Revised : 2024. 08. 23.
Accepted : 2024. 08. 29.